Bull. Mater. Sci., Vol. 38, No. 1, February 2015, pp. 163–167. © Indian Academy of Sciences.

A sensitive nonenzymatic hydrogen peroxide sensor based on Fe_3O_4–Fe_2O_3 nanocomposites

GUANG SHENG CAO*, PEILONG WANG, XIN LI, YUE WANG, GUILONG WANG and JUNPING LI

Key Laboratory of Enhanced Oil & Gas Recovery of Ministry of Education, Northeast Petroleum University, Daqing 163318, PR China

MS received 31 January 2014; revised 12 April 2014

Abstract. **The Fe_3O_4–Fe_2O_3 nanocomposites were prepared by the co-precipitation method and followed by calcination process. The products were synthesized and characterized by X-ray diffraction, scanning electron microscopy, transmission electron microscopy and energy-dispersive X-ray analysis. The obtained Fe_3O_4–Fe_2O_3 nanocomposites were then applied to study the electrocatalytic reduction of hydrogen peroxide (H_2O_2) in 0.01 M pH 7.0 phosphate buffer medium. Then the Fe_3O_4–Fe_2O_3 nanocomposites were used as active electrode material of electrochemical sensors for H_2O_2 detection The detection sensitivity of the sensor was 20.325 μA mM^{-1}, and the detection limit was estimated to be about 0.2 mM.**

Keywords. **Fe_3O_4; Fe_2O_3; nanocomposites; hydrogen peroxide; sensor.**

1. Introduction

Owing to its strong oxidizing property, hydrogen peroxide (H_2O_2) is widely used in many fields. For example, H_2O_2 is useful for food production, sterilization, clinical applications and environmental analyses.[1–4] Further, H_2O_2 has emerged as an important by-product of enzymatic reactions in the field of biosensing. Thus, accurate and reliable determination of H_2O_2 has been widely investigated using spectrometry, chemiluminescence and electrochemistry technologies.[5–7] Among these methods, electrochemical method has been extensively applied due to its simple, accurate and fast analytical process. Many enzyme-based electrochemical biosensors towards H_2O_2 reduction have been made. However, the immobilized enzyme/protein on the surface of the electrode is facilitated to denature, which leads to such modified electrodes that suffer from a poor enzyme/protein activity, a low reproducibility and stability.[8] Nanomaterials can play an important role in improving sensor performance, due to their large specific surface areas, excellent conductivities and compatibilities. In recent years, nanomaterials have been regarded as excellent substitutes for enzymes. Single crystal and vertically aligned Co_3O_4 nanowalls were synthesized, and the Co_3O_4 nanowall electrode was applied for the amperometric detection of H_2O_2 and showed a fast response and high sensitivity.[9] Gu *et al*[10] have synthesized Cu–$Ni(OH)_2$ nanocomposites and applied it as the fast and sensitive H_2O_2 sensor material. Ag nanoparticles were synthesized on indium tin oxide conducting glass substrate using the electrochemical deposition method, and the developed Ag nanoparticles sensor had excellent electrocatalytic activity for H_2O_2 detection.[11] The electrocatalytic activity of CuO flower-like nanostructured electrode was investigated in terms of its application to enzymeless amperometric H_2O_2 sensors.[12]

Transition metal oxide nanomaterials are one of the promising candidates for the active electrode material of non-enzymatic electrochemical sensors. Magnetite (Fe_3O_4), which is chemically stable, non-toxic and non-carcinogenic, has a high magnetic saturation value.[13–15] Hematite (α-Fe_2O_3), the most stable iron oxide under ambient condition with low-cost, non-toxicity and environmental-friendly features, is of great scientific and technology importance.[16] Fe_3O_4 and Fe_2O_3 have been widely fabricated as gas sensor because of its good stability, lower cost and easy availability. Yu *et al*[17] reported the application of chitosan–Fe_3O_4 nanocomposite-modified glassy carbon electrodes for the amperometric determination of bisphenol A. A novel imprinted sol–gel electrochemical sensor based on multi-walled carbon nanotubes doped with chitosan film on a carbon electrode has been developed.[18] La-doped Fe_2O_3 nanotubes are synthesized by an electrospinning method and followed by calcination, and the nanotubesshow a good selectivity to acetone.[19] To the best of our knowledge, H_2O_2 electrochemical sensor based on the Fe_3O_4–Fe_2O_3 nanocomposites has never been reported before. In this study, Fe_3O_4–Fe_2O_3 nanocomposites are synthesized by the co-precipitation method and followed by calcination process. The Fe_3O_4–Fe_2O_3 nanocomposites

*Author for correspondence (daqingcgs@163.com)

were applied for the sensitive amperometric detection of H_2O_2. The proposed sensor possesses high sensitivity and high stability.

2. Experimental

2.1 *Sample preparation*

Fe_3O_4–Fe_2O_3 nanocomposites were synthesized by the co-precipitation method and followed by calcination. Typically, 2.2 g of $FeCl_3 \cdot 6H_2O$ and 2.3 g of $FeSO_4 \cdot 7H_2O$ were dissolved in 30 ml of 0.01 M HCl to form a transparent solution. When the solution became clear, the mixture was then added drop-wise to 40 ml of 3 M $NH_3 \cdot H_2O$ with the reaction mixture vigorously stirred at 80°C for 150 min. The final products were collected, followed by calcination at 350–500°C for 4 h.

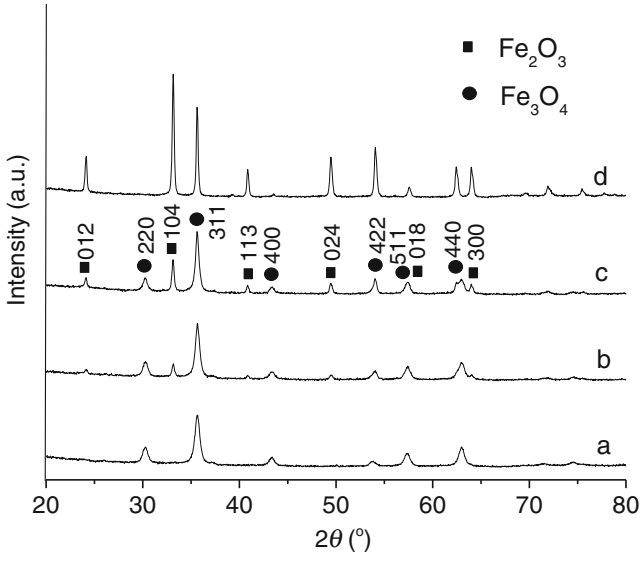

Figure 1. XRD patterns of products synthesized at different calcination temperatures: **(a)** 350°C, **(b)** 400°C, **(c)** 450°C and **(d)** 500°C.

2.2 *Electrode preparation*

Glassy carbon (GC) disks were polished with 0.03 mm Al_2O_3 powders. A typical suspension of the Fe_3O_4–Fe_2O_3 nanocomposites was prepared by suspending 6 mg Fe_3O_4–Fe_2O_3 nanocomposites in 3 ml 0.5% Nafion solution, and sonicated for 15 min. The suspension was transferred to the surface of the polished GC disk and dried at 80°C for 5 min.

2.3 *Characterization*

Scanning electron microscopy (SEM, Hitachi S-4700) was used to characterize the morphology of the Fe_3O_4–Fe_2O_3 nanocomposites. The chemical compositions of the products were detected using an energy-dispersive X-ray spectrometry (EDS, Thermo Noran VANTAG-ESI). The obtained samples were characterized by X-ray powder diffraction (XRD) using a Rigaku D/max-γB X-ray diffractometer with graphite monochromatized Cu Kα radiation ($\lambda = 1.54178$ Å) operated at 40 kV and 80 mA. Electrochemical measurements were performed using a computer-controlled CHI 660C electrochemical workstation in a standard three-electrode configuration, including Fe_3O_4–Fe_2O_3 nanocomposite electrodes as the working electrode, an Ag/AgCl reference electrode and a platinum counter electrode. H_2O_2 measurement was carried out in 0.01 M, pH 7.0, phosphate buffer containing 0.2–1.8 mM H_2O_2.

3. Results and discussion

In our study, the calcination temperature is varied from 350 to 450°C to investigate its influence on the structure. Figure 1a shows the XRD patterns of the as-obtained products at 350°C. All the diffraction peaks in figure 1a can be readily indexed to Fe_3O_4 of spinel structure (JCPDS Card no. 19-0629). Figure 1b shows the XRD pattern of the as-obtained product at 400°C. All of the peaks of the XRD pattern in figure 1b can be indexed to a mixed phase of Fe_3O_4 (JCPDS Card no. 19-0629) and α-Fe_2O_3 (JCPDS Card no.

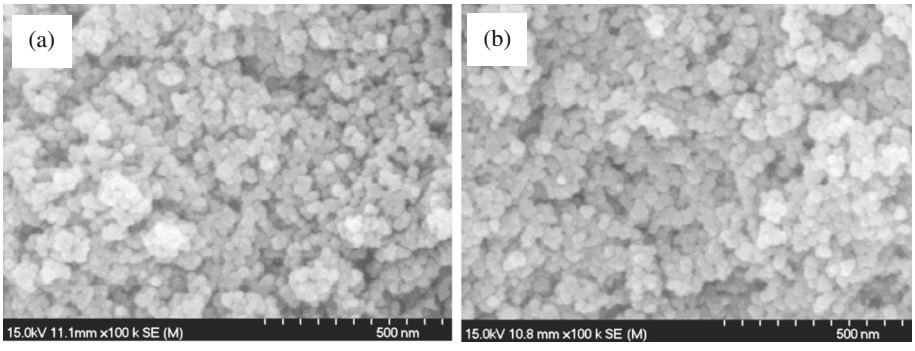

Figure 2. SEM images of the Fe_3O_4–Fe_2O_3 nanocomposites prepared at **(a)** 400°C and **(b)** 450°C.

39-1346). This reveals that Fe_3O_4–Fe_2O_3 composites were obtained at 400°C. When calcination temperatures are above 450°C, it can be easily found from figure 1c that besides the diffraction peaks of Fe_3O_4, strong diffraction peaks of α-Fe_2O_3 are observed. Figure 1d shows the XRD patterns of the as-synthesized samples at 500°C, all the reflection peaks can be readily indexed to α-Fe_2O_3 (JCPDS Card no. 39-1346). The XRD patterns indicate that Fe_3O_4–Fe_2O_3 composites were obtained in the calcination temperature range under investigation (350–450°C).

The morphologies of the as-obtained products were examined by SEM microscopy. Figure 2a shows the pattern of the Fe_3O_4–Fe_2O_3 composites prepared at 400°C. The SEM image displayed much smaller nanoparticles with diameters of about 40–50 nm. Figure 2b is the SEM image of the sample prepared at 450°C. SEM images revealed that the morphologies of the Fe_3O_4–Fe_2O_3 nanocomposites prepared at 450°C were similar to the sample prepared at 350°C.

HRTEM analysis provides more detail structural information about the Fe_3O_4–Fe_2O_3 nanocomposites, showing the apparent lattice fringes of the crystal. Figure 3 is an HRTEM image taken from the Fe_3O_4–Fe_2O_3 nanocomposites. The observed interplanar spacing is 0.309 and 0.205 nm, which correspond to the (012) atomic spacing of Fe_3O_4 and the (400) atomic spacing of Fe_2O_3, respectively.

The EDS patterns of the Fe_3O_4–Fe_2O_3 nanocomposites prepared at 400 and 450°C are shown in figure 4. It can be seen that the main elements in the samples are O and Fe and the peak intensity of Fe decreases with the increasing calcination temperature. Fe and O elements existed in the Fe_3O_4–Fe_2O_3 nanocomposites prepared at 400 and 450°C have the molar ratio of 72.9:100 and 70.6:100, respectively. By calculation, the Fe_3O_4–Fe_2O_3 molar ratios in the Fe_3O_4–Fe_2O_3 nanocomposites are 2.22:1 and 0.67:1.

The electrocatalytic activity of the as-obtained products at different calcination temperature was studied. All samples exhibited the reduction of H_2O_2 starting around −0.5 V. The Fe_3O_4–Fe_2O_3 nanocomposites prepared at 400°C exhibited the strongest electrocatalytic ability towards the reduction of H_2O_2. The electro-reduction mechanism of H_2O_2 on

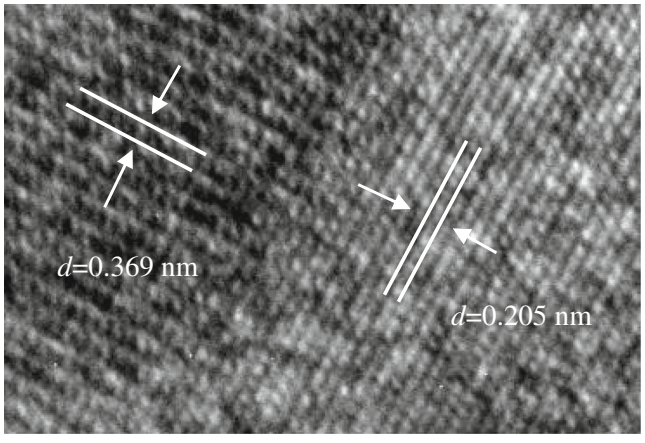

Figure 3. HRTEM images of the Fe_3O_4–Fe_2O_3 nanocomposites.

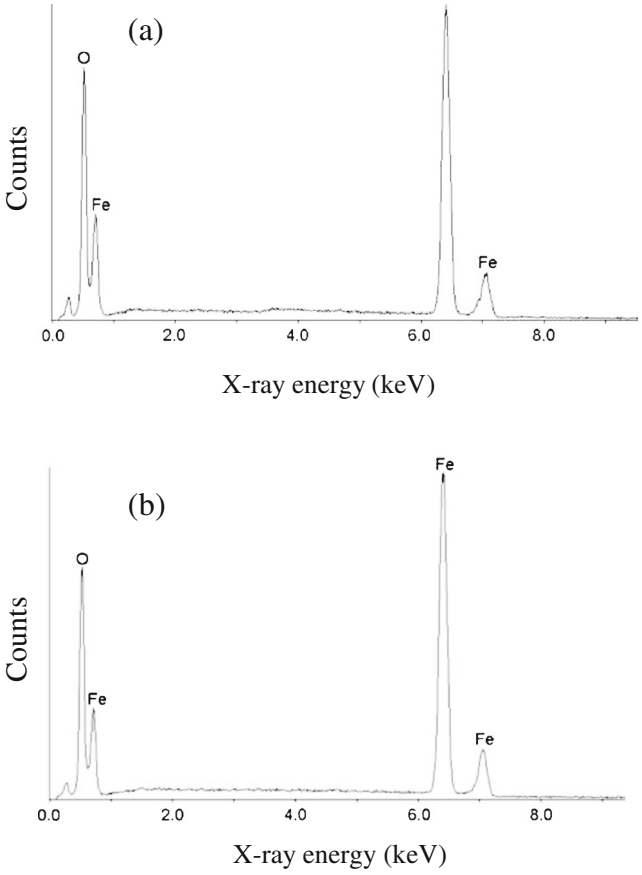

Figure 4. EDS patterns of the Fe_3O_4–Fe_2O_3 nanocomposites prepared at **(a)** 400°C and **(b)** 450°C.

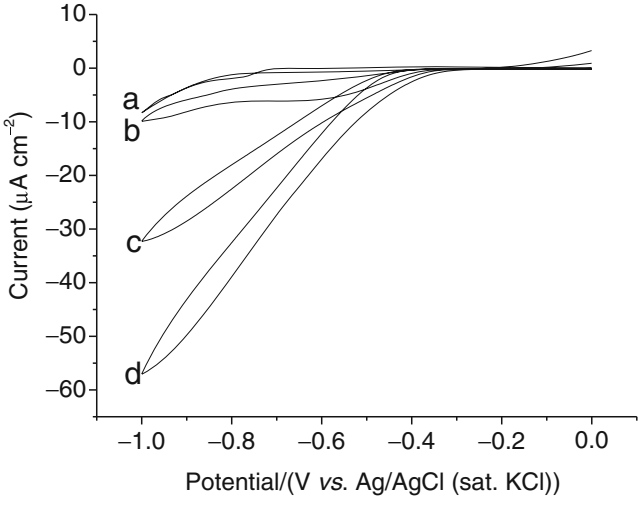

Figure 5. CV of the Fe_3O_4–Fe_2O_3 nanocomposites at various concentrations of H_2O_2: **(a)** 0 mM, **(b)** 0.2 mM, **(c)** 0.6 mM and **(d)** 1.0 mM.

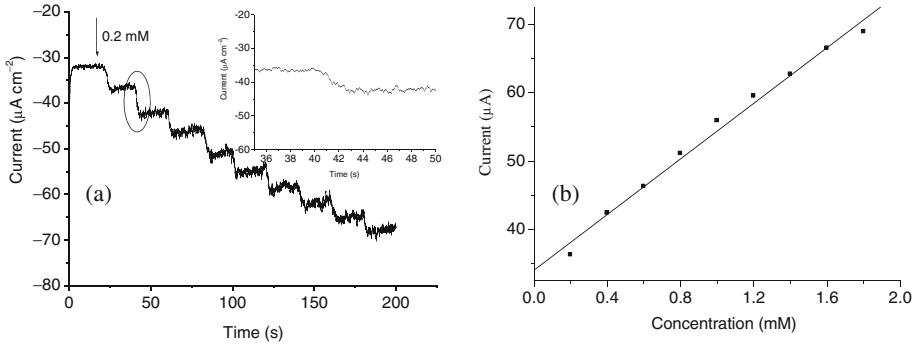

Figure 6. **(a)** Amperometric current response of the Fe_3O_4–Fe_2O_3 nanocomposite electrodes on the successive injection of H_2O_2 with various concentrations into stirring 0.01 M phosphate buffer and **(b)** calibration curve of H_2O_2 concentration on the electrode.

the Fe_3O_4–Fe_2O_3 nanocomposites can be illustrated by the equations below

$$Fe_3O_4 + H_2O_2 \rightarrow Fe_2O_3 + OH^-, \quad (1)$$

$$Fe_2O_3 + H_2O + e^- \rightarrow Fe_3O_4 + OH^-. \quad (2)$$

Based on the XRD, HRTEM and FDS analysis, it is obvious that the strongest electrocatalytic activity of the Fe_3O_4–Fe_2O_3 nanocomposites may be attributed to its structure with the interface of Fe_3O_4–Fe_2O_3. According to the mechanism above, the reaction exists in Fe_3O_4 and Fe_2O_3. In Fe_3O_4–Fe_2O_3 nanocomposites, there are many Fe_3O_4–Fe_2O_3 interfaces, which is favourable for increasing diffusion rate and accelerating electrode kinetics. It is believed that the structure and Fe_2O_3 content have played an important role in controlling the reduction of H_2O_2.

Figure 5 shows the CVs of the Fe_3O_4–Fe_2O_3 nanocomposites prepared at 400°C in 0.01 M phosphate buffer containing H_2O_2 with different concentrations. The current sensitivity increases with increasing H_2O_2 concentration (from the top: 0, 0.2, 0.6, 1.0 mM), which may be applied as the quantitative analysis. Figure 6a displays a typical current–time plot of the Fe_3O_4–Fe_2O_3 nanocomposites on the successive addition of H_2O_2 with various concentrations into stirring phosphate buffer (0.01 M, pH 7.0) at the applied potential of −1.0 V. These Fe_3O_4–Fe_2O_3 nanocomposite sensors show a very fast response, as the response reaches 100% of the steady-state value within 2.5 s. The calibration curves of the Fe_3O_4–Fe_2O_3 nanocomposites sensor are shown in figure 6b. The sensor has a wide linear range from 0.2 to 1.8 mM with a correlation coefficient of 0.997, and the sensitivity is determined to be as 20.325 μA mM^{-1}. The selectivity of the sensor was also evaluated with four species: SO_4^{2-}, Cl^-, ClO_3^- and CO_3^{2-}. When SO_4^{2-}, Cl^-, ClO_3^- and CO_3^{2-} were injected into the phosphate buffer, no obvious current was observed as shown in figure 7. This suggests that these species have no obvious interference in the reduction of H_2O_2.

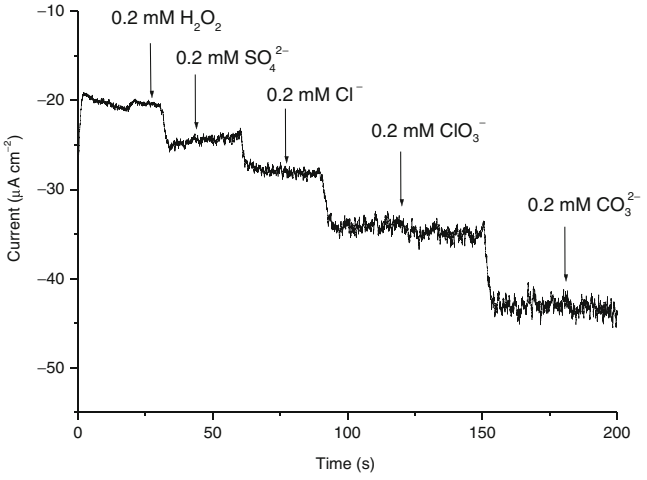

Figure 7. Current responses of the Fe_3O_4–Fe_2O_3 nanocomposites to sequential additions of H_2O_2, SO_4^{2-}, Cl^-, ClO_3^{2-} and CO_3^{2-} in 0.01 M phosphate buffer.

4. Conclusion

In conclusion, the Fe_3O_4–Fe_2O_3 nanocomposites have been successfully synthesized by the co-precipitation method and followed by calcination process. The electrocatalytic activity of the as-obtained products at different calcination temperatures was studied by CV. It was found that the Fe_3O_4–Fe_2O_3 nanocomposites obtained at 400°C showed maximal electrocatalytic ability for the reduction of H_2O_2. The amperometric response of the electrode was rapid (within 2.5 s), and had high sensitivity (20.325 μA mM^{-1}). The proposed electrochemical sensor based on Fe_3O_4–Fe_2O_3 nanocomposites is thus expected to generate new opportunities for monitoring H_2O_2 concentrations in industry analyses fields.

References

1. Klassen N V, Marchington D and Mcgowan H C E 1994 *Anal. Chem.* **66** 2921

2. Salimi A, Hallaj R, Soltanian S and Mamkhezri H 2007 *Anal. Chim. Acta* **594** 24
3. Yang Y J and Hu S 2010 *Electrochim. Acta* **55** 3471
4. Song X C, Wang X, Zheng Y F, Ma R and Yin H Y 2011a *J. Nanopart. Res.* **13** 1319
5. Diaz A N, Peinado M C R and Minguez M C T 1998 *Anal. Chim. Acta* **363** 221
6. Tanner P A and Wong A Y S 1998 *Anal. Chim. Acta* **370** 279
7. Cui K, Song Y H, Yao Y, Huang Z Z and Wang L 2008 *Electrochem. Commun.* **10** 663
8. Miao X, Yuan R, Chai Y, Shi Y and Yuan Y 2008 *J. Electroanal. Chem.* **612** 157
9. Jia W, Guo M, Zheng Z, Yu T, Rodriguez E G, Wang Y and Lei Y 2009 *J. Electroanal. Chem.* **625** 27
10. Gu A, Wang G, Gua J, Zhang X and Fang B 2010 *Electrochim. Acta* **55** 7182
11. Song X C, Wang X, Zheng Y F, Ma R and Yin H Y 2011b *J. Nanopart. Res.* **13** 5449
12. Song M, Hwang S W and Whang D 2010 *Talanta* **80** 1648
13. Tural B, Ozkan N and Volkan M 2009 *J. Phys. Chem. Solids* **70** 860
14. Wang N, Zhu L, Wang M, Wang D and Tang H 2010 *Ultrasonics Sonochem.* **17** 78
15. Song X C, Zheng Y F and Yin H Y 2013 *J. Nanopart. Res.* **15** 1856
16. Wang Y, Cao J, Yu M, Sun G, Wang X, Bala H and Zhang Z 2013 *Mater. Lett.* **100** 102
17. Yu C, Gou L, Zhou X, Bao N and Gu H 2011 *Electrochim. Acta* **56** 9056
18. Hu Y, Li J, Zhang Z, Zhang H, Luo L and Yao S 2011 *Anal. Chim. Acta* **698** 61
19. Shan H, Liu C, Liu L, Li S, Wang L, Zhang X, Bo X and Chi X 2013 *Sens. Actuators B* **184** 243